

DERIVATIVE-INFORMED PROJECTED NEURAL NETWORKS FOR HIGH-DIMENSIONAL PARAMETRIC MAPS GOVERNED BY PDES*

THOMAS O'LEARY-ROSEBERRY[†], UMBERTO VILLA[‡], PENG CHEN^{*}, AND
OMAR GHATTAS[§]

Abstract. Many-query problems—arising from, e.g., uncertainty quantification, Bayesian inversion, Bayesian optimal experimental design, and optimization under uncertainty—require numerous evaluations of a parameter-to-output map. These evaluations become prohibitive if this parametric map is high-dimensional and involves expensive solution of partial differential equations (PDEs). To tackle this challenge, we propose to construct surrogates for high-dimensional PDE-governed parametric maps in the form of derivative-informed projected neural networks (DIPNets) that parsimoniously capture the geometry and intrinsic low-dimensionality of these maps. Specifically, we compute Jacobians of these PDE-based maps, and project the high-dimensional parameters onto a low-dimensional derivative-informed active subspace; we also project the possibly high-dimensional outputs onto their principal subspace. This exploits the fact that many high-dimensional PDE-governed parametric maps can be well-approximated in low-dimensional parameter and output subspaces. We use the projection basis vectors in the active subspace as well as the principal output subspace to construct the weights for the first and last layers of the neural network, respectively. This frees us to train the weights in only the low-dimensional layers of the neural network. The architecture of the resulting neural network then captures, to first order, the low-dimensional structure and geometry of the parametric map. We demonstrate that the proposed projected neural network achieves greater generalization accuracy than a full neural network, especially in the limited training data regime afforded by expensive PDE-based parametric maps. Moreover, we show that the number of degrees of freedom of the inner layers of the projected network is independent of the parameter and output dimensions, and high accuracy can be achieved with weight dimension independent of the discretization dimension.

Key words. Deep learning, neural networks, parametrized PDEs, derivative-informed dimension reduction, active subspace, proper orthogonal decomposition, surrogate modeling, adjoint-based sensitivity, Hessian, uncertainty quantification.

AMS subject classifications. 49M41, 65C20, 93E20, 93E35

1. Introduction. Many problems in computational science and engineering require repeated evaluation of an expensive nonlinear parametric map for numerous instances of input parameters drawn from a probability distribution ν . These *many-query problems* arise in such problems as Bayesian inference, forward uncertainty quantification, optimization under uncertainty, and Bayesian optimal experimental design (OED), and are often governed by partial differential equations (PDEs). The maps are parameterized by model parameters m with joint probability distribution ν , which is mapped to outputs q through an implicit dependence on the solution of the PDEs for the state u :

$$(1.1) \quad \underbrace{q(m) = q(u(m))}_{\text{Implicit dependence}} \text{ where } u \text{ depends on } m \text{ through } \underbrace{R(u, m) = 0}_{\text{PDE model}}$$

*This research partially supported by ARPA-E DIFFERENTIATE grant DE-AR0001208; NSF SI2-SSI grant ACI-1550593; DOE ASCR MMICC grant DE-SC0019303; and NSF DMS grant 2012453.

[†]Oden Institute for Computational Engineering & Sciences, The University of Texas at Austin, Austin, TX (tom@oden.utexas.edu, peng@oden.utexas.edu).

[‡]McKelvey School of Engineering, Washington University in St. Louis, Saint Louis, MO (uvilla@wustl.edu).

[§]Oden Institute for Computational Engineering & Sciences, Jackson School of Geosciences, and Department of Mechanical Engineering, The University of Texas at Austin, Austin, TX (omar@oden.utexas.edu).

The variables $m \in \mathbb{R}^{d_M}$, $u \in \mathbb{R}^{d_U}$ are formally discretizations of functions in Banach spaces, where the dimensions d_M and d_U are often large. We assume that the outputs $q \in \mathbb{R}^{d_Q}$ are differentiable with respect to m . The outputs can be the full PDE states u , or state dependent quantity of interest, such as integrals or (mollified) pointwise evaluations of the states or their fluxes, as arise in inverse problems, optimal design and control, and OED.

Each evaluation of q requires solution of the PDEs at one instance of m , thus making solution of many-query problems prohibitive when the solution of the governing PDEs is expensive due to nonlinearity, multiphysics or multiscale nature, and/or complex geometry. For example, solution of complex PDEs can take hours or even days or weeks on a supercomputer, making the solution of many-query problems prohibitive using the full high fidelity PDE solution.

Thus, practical solution of high dimensional many-query problems requires surrogates for the mapping $m \mapsto q$. The goal of surrogate construction is to construct approximations of the map that are accurate over the probability distribution for input parameters, ν , i.e., to find a surrogate $f \in \mathbb{R}^{d_Q}$ that is inexpensive to construct and evaluate and that satisfies

$$(1.2) \quad \mathbb{E}_\nu[\|q - f\|^2] = \int \|q(m) - f(m)\|^2 d\nu(m) < \epsilon$$

for a suitable tolerance $\epsilon > 0$, in a suitable norm. Here \mathbb{E}_ν is the expectation with respect to ν , as defined in equation (1.2).

To tackle this challenge, various forms of surrogates have been developed that exploit intrinsic properties of the high-dimensional parameter-to-output map, $m \mapsto q$ such as sparsity and low-dimensionality, including, e.g., sparse polynomials [6, 25, 33, 68], and reduced basis methods [19, 27, 28, 33]. Dimension-independent complexity to achieve a desired accuracy has been shown for these methods under suitable assumptions; see the review in [33] and references therein. In recent years, neural networks have shown great promise in representing high dimensional nonlinear mappings, especially in data-rich applications such as computer vision and natural language processing; see for example [39]. In these regimes neural networks with high weight dimensions can learn patterns in very large data sets. More recently, significant interest has arisen in using neural networks as nonlinear surrogates for PDE-governed high-dimensional parametric maps in the many-query setting [9, 41, 60, 62, 71].

However, the PDE-governed many-query regime is fundamentally different from the data-rich regime of typical data science problems. The key difference is that in the former, few data may be available to train a surrogate due to the expense of evaluating the map, and the input–output pairs may be very high dimensional. For example, consider a high parameter dimension climate model: the parameters (e.g., unknown initial conditions) and outputs (e.g., future states) may number in the millions or billions, but one can afford only hundreds of evaluations of the mapping $m \mapsto q$. Because the number of weights in a dense neural network model would then scale with the square of the number of parameters/outputs, the number of climate model runs needed to fully inform the weights would need to scale with the number of parameters and outputs. This is orders of magnitude larger than is feasible. Black box strategies for dimension reduction such as convolution kernels can efficiently represent discretizations of stationary processes on regular (Cartesian) grids. The limitation to regular grids presents difficulties for many PDE problems discretized on highly unstructured meshes. Recent works in geometric deep learning have extended convolution processes to non-Cartesian data [11, 51], but even when the meshes are uniform, the question

of finding the right architecture remains, as does the question of associated dimension reduction. Genetic algorithms can be used to select neural network architectures [10, 63, 69], but this can be prohibitive, since each proposed network needs to be trained in order to test its viability, and the number of trained networks that need to be explored will be large due to the heuristic nature of these algorithms.

The key idea for overcoming this critical challenge faced by the PDE-governed setting is that the mapping $m \mapsto q$ often has low-dimensional structure and smoothness that can be exploited to aid architecture selection as well as provide informed subspaces of the input and intrinsic subspaces of the outputs, within which the mapping can be well approximated. This intrinsic low-dimensionality is revealed by the Jacobian and higher-order derivatives of q with respect to m . This has been proven for certain model problems and demonstrated numerically for many others in model reduction [5, 7, 21], Bayesian inversion [12, 14, 15, 16, 17, 18, 22, 29, 32, 37, 43, 49, 57], optimization under uncertainty [4, 23, 24, 30], and Bayesian optimal experimental design [2, 3, 35, 67].

In this work we consider strategies for constructing reduced dimension projected neural network surrogates using Jacobian-based derivative information for effective input dimension reduction, and represent the outputs in their principal subspace. The resulting networks can be viewed as encoder-decoder networks with a priori computed reduced input and output bases that reflect the geometry and low-dimensionality of the parameter-to-output map. When the bases for the inputs and outputs are fixed, the weight dimension of the neural network is independent of the discretization dimensions of the PDE model. On the other hand, when these bases are permitted to be modified during neural network training, they serve as good initial guesses that impose the parametric map’s structure on the full encoder-decoder training problem.

We consider active subspaces (AS) [34, 70] for the input space reduction, and the principal subspace given by proper orthogonal decomposition (POD) [48, 59] for the output reduction. AS incorporates Jacobian information to detect input subspaces to which the outputs are sensitive, while POD provides a low dimensional subspace in which the outputs are efficiently represented, we call this neural network strategy DIPNet (derivative informed projected neural network). We compare this strategy to the use of Karhunen Loève expansion (KLE) projections for the input space and POD for the output projection, as was done in [9]. KLE exploits low dimensionality of the parameter probability distribution, as exposed by the eigenvalue decay of its covariance operator, but does not account for the outputs. KLE and POD are related to principal component analysis (PCA) of the parameter data and output data respectively. PCA is a popular strategy for dimension reduction in neural network architecture selection; see for example [38]. We favor the AS for the input projection, since it is derivative-informed; AS explicitly incorporates the sensitivity of the outputs to the inputs in determining the dimension reduction.

To motivate this strategy, we derive an input–output projection error bound based on optimal ridge functions for Gaussian parametric mappings. We construct DIPNet surrogates based on AS-to-POD neural network ridge functions, which we compare against KLE-to-POD neural network ridge functions as well as conventional approaches using full space neural networks.

We test the resulting surrogates on two different PDE parameter-to-output map problems: one parametric mapping involving pointwise observations of the state for a nonlinear convection-diffusion-reaction problem, and another involving a high frequency Helmholtz problem. We consider problems where d_M is large, but d_Q is smaller; thus, we keep the first layer fixed but train the output layer. These numer-

ical experiments demonstrate that full space neural network surrogates that depend on the dimension of the discretization parameter perform poorly in generalization accuracy in the low data regime. On the other hand, the projected neural network surrogates are capable of achieving high accuracy in the low data regime; in particular the DIPNet strategy performs best. We also test against neural network ridge functions with identical architectures that instead use Gaussian random projection bases to test the effect of the structured bases (DIPNet and KLE-to-POD), and demonstrate that the random projections performs worse than the structured ones.

Contributions: We propose a general framework to construct surrogates for high-dimensional parameter-to-output maps governed by PDEs in the form of derivative-informed low-dimensional projected neural networks (DIPNets) that generalize well even with limited numbers of training data. This framework exploits informed input and output subspaces that reveal the intrinsic dimensionality of the parameter-to-output map. The strategy involves constructing ridge function surrogates that attempt to learn only the nonlinear mapping between informed modes of the input parameters and output spaces. This strategy is infinite-dimensionally consistent since the operators used in the neural network construction are mesh independent.

Our work differs from [9], which uses KLE-based input projections; instead, we use derivative-informed active subspace-based projections. Both representations have input–output projection error bounds given respectively by the eigenvalue decays of the AS, KLE, and POD operators. For a fixed rank ridge function surrogate, the bounds for the AS-to-POD surrogates are tighter than those for the KLE-to-POD, which involve the square of the Lipschitz constant for the parameter-to-output map. These are conservative upper bounds, but one can reasonably expect that incorporating specific information about the outputs in the input basis can provide better accuracy with fewer modes. This is confirmed in numerical experiments.

Numerical experiments demonstrate that the DIPNet strategy using AS performs well in the limited data regime typical of PDE-governed parametric maps. When the squared Jacobian of the parameter-to-output map has spectral structure similar to the covariance operator of the input parameter distribution, the KLE eigenvectors perform well as a reduced basis—nearly as well as the AS strategy. When the parameter-to-output map differs from the covariance operator, the KLE strategy is seen to perform worse than the AS strategy, and only slightly better than using Gaussian random bases.

The rest of the paper is organized as follows: In Section 2, we discuss techniques for input-output dimension reduction for parametric maps, and derive an input–output projection error bound based on optimal ridge functions for Gaussian parametric mappings based on AS, KLE and POD. In Section 3 we present strategies for constructing DIPNet surrogates using these building blocks, and discuss errors incurred in the surrogate construction procedure. In Section 4 we present numerical experiments that demonstrate the viability of the derivative-informed projected neural network approach for two problems arising from parametric PDE inference problems.

2. Input-Output Projected Ridge Function Surrogates. We proceed by discussing strategies for input-output projected ridge functions of the form

$$(2.1) \quad q(m) \approx f(m) = \Phi_{r_Q} f_r(V_{r_M}^T m) + b_Q,$$

where V_{r_M} are a reduced basis for the input space, Φ_{r_Q} are a reduced basis for the outputs, and $f_r : \mathbb{R}^{r_M} \rightarrow \mathbb{R}^{d_Q}$ is a ridge function. We begin by examining strategies

for input and output projection, and known bounds for projection errors, which lead to an input–output bound that motivates our general approach.

2.1. Input Projection: Active Subspace and Karhunen-Loève Expansion. In the setting of parametric mappings, the input parameters m come from a discretization of an infinite dimensional parameters. Algorithmic complexity suffers from the curse of dimensionality as the discretization dimension grows. In order to avoid the curse of dimensionality we seek to exploit low-dimensional structure of the parameter-to-output map in architecting neural network surrogates.

An effective strategy for constructing an input dimension reduced surrogate is to construct an optimal ridge function approximation of $m \mapsto q$. A ridge function is a composition of the form $g \circ h$, where $h : \mathbb{R}^{d_M} \rightarrow \mathbb{R}^r$ is a linear mapping (a tall skinny matrix, with $r \ll d_M$), and $g : \mathbb{R}^r \rightarrow \mathbb{R}^{d_Q}$ is a measurable function in $L^2(\mathbb{R}^{d_M}, \sigma(h), \mathbb{R}^{d_Q})$, i.e. in the σ -algebra generated by the bases of h . Input dimension reduced dense neural networks have this form.

We seek to construct ridge function surrogates for the mapping $m \mapsto q$ that are restricted to subspaces of the input space that resolve intrinsic low dimensionality about the mapping. The goal is to find a (nonlinear) ridge function g and a linear projector of dimension r , $V_r : \mathbb{R}^{d_M} \rightarrow \mathbb{R}^r$ such that for a given tolerance $\epsilon > 0$,

$$(2.2) \quad \mathbb{E}_\nu[\|q - g \circ V_r\|_X] \leq \epsilon$$

in a suitable norm X . The key issues that remain are how to find V_r , i.e. both the dimension r and the subspace $X_r \subset \mathbb{R}^{d_M}$ spanned by the column bases of V_r .

One approach we consider is to use Karhunen-Loève expansion (KLE) [61], which exploits low dimensional correlation structure of the probability distribution ν of the parameters m . This approach is equivalent to principal component analysis (PCA) of input data. It is considered for solving parametric PDEs using dimension reduced neural networks in [9].

For a Gaussian distribution $\nu = \mathcal{N}(m_0, C)$, with mean $m_0 \in \mathbb{R}^{d_M}$ and covariance $C \in \mathbb{R}^{d_M \times d_M}$, the optimal rank r basis $V_r \in \mathbb{R}^{d_M \times r}$ for representing samples $m_i \sim \nu$ is given by the r eigenvectors corresponding to the r biggest eigenvalues of the covariance matrix $C = \Psi \text{diag}(c) \Psi^T$, with $(c_i, \Psi_i)_{i \geq 1}$ representing the eigenpairs of C ordered such that $c_1 \geq c_2 \geq \dots \geq c_{d_M} \geq 0$, i.e

$$(2.3) \quad \min_{V_r \in \mathbb{R}^{d_M \times r}} \mathbb{E}_{m_i \sim \nu}[\|(I_d - V_r V_r^T)(m_i - m_0)\|_2^2] = \sum_{i=r+1}^{d_M} c_i^2.$$

See [70].

The input data are restricted to the dominant modes of the covariance of the parameter distribution ν . This approach is appropriate in regimes where the output variability is dominated by the parameter variability in the leading input modes, and the parameter covariance has rapidly decaying eigenvalues.

Input dimension reduction using KLE has limitations since it does not explicitly take into account the mapping $m \mapsto q$, it is only dependent on the distribution ν . For this reason we propose to use derivative-informed input dimension reduction based on the map Jacobian information. The Jacobian of the outputs with respect to the parameters can be used to find a global subspace in which the outputs are most sensitive to the input parameters over the parameter space. Similar techniques have been popularized for dimension reduction for scalar valued functions under the name “active subspaces” (AS) [34], for which projection error bounds can be established

using Poincaré inequalities. The ideas have been generalized to vector valued functions [70], or scenarios where Poincaré inequalities do not hold [56].

The active subspace is constructed by the eigenvectors of the Jacobian information matrix, or a Gauss-Newton Hessian of $\frac{1}{2}\|q(m)\|_{\ell^2(\mathbb{R}^{d_Q})}^2$ averaged with respect to the parameter distribution, i.e.,

$$(2.4) \quad H_{\text{GN}} = \mathbb{E}_\nu[\nabla q^T \nabla q] = \int_M \nabla q(m)^T \nabla q(m) d\nu(m) \in \mathbb{R}^{d_M \times d_M}.$$

The leading eigenvectors corresponding to the largest eigenvalues of H_{GN} represents directions in which the parameter-to-output map $m \mapsto q$ is most sensitive to the input parameters $m \in \mathbb{R}^{d_M}$ in the $\ell^2(\mathbb{R}^{d_Q})$ sense (i.e. as informs a regression problem).

Consider the ridge function parametrizations given by the $g(P_r m)$, where $P_r \in \mathbb{R}^{d_M \times d_M}$ is a rank- r projector. In [70] upper bounds are established for the approximation error of $m \mapsto q$ using a conditional expectation of q with restricted to the dominant modes of the averaged Gauss-Newton Hessian (Equation 2.4). Specifically let $(\lambda, v_i)_{i \geq 1}$ denote the eigenpairs of the generalized eigenvalue problem

$$(2.5) \quad H_{\text{GN}} v_i = \lambda_i C^{-1} v_i,$$

then an upper bound for the approximation error $\|q - \mathbb{E}_\nu[q|\sigma(P_r)]\|_{\mathcal{H}}^2$ can be obtained (see Proposition 2.6 in [70]):

$$(2.6) \quad \|q - \mathbb{E}_\nu[q|\sigma(P_r)]\|_{\mathcal{H}}^2 \leq \sum_{i=r+1}^{d_M} \lambda_i^M,$$

when the projector is taken to be

$$(2.7) \quad P_r = V_r V_r^T C^{-1}.$$

Here the function space $\mathcal{H} = L^2(\mathbb{R}^{d_M}, \nu; \mathbb{R}^{d_Q})$, and the \mathcal{H} norm is induced by the inner product:

$$(2.8) \quad (u, v)_{\mathcal{H}} = \int_{\mathbb{R}^{d_M}} (u(m), v(m))_{\ell^2(\mathbb{R}^{d_Q})} d\nu(m).$$

The conditional expectation $\mathbb{E}_\nu[q|\sigma(P_r)](m)$ represents the mapping $m \mapsto q$ with orthogonal complement to $\text{span}\{P_r\}$ in the parameter space marginalized out. In the case that the projector P_r is orthogonal with respect to the covariance C , the conditional expectation with respect to the σ -algebra generated by P_r can be written as

$$(2.9) \quad \mathbb{E}_\nu[q|\sigma(P_r)](m) = \mathbb{E}_{y \sim \nu}[q(P_r m + (I_{d_M} - P_r)y)].$$

This bound establishes that when the spectrum of the Gauss-Newton Hessian decays rapidly, the mapping $m \mapsto q$ can be well approximated in expected value by the conditional expectation $\mathbb{E}_\nu[q|\sigma(P_r)](m)$, which is marginalized to the subspace spanned by the dominant modes of H_{GN} .

When the mapping q is Lipschitz continuous with constant $L \geq 0$, and the eigenvalues of the parameter distribution covariance decay quickly, the KLE can be used to construct a similar ridge function bound, i.e. there exist a function g and projector P_r such that

$$(2.10) \quad \|q - g \circ P_r\|_{\mathcal{H}}^2 \leq L^2 \sum_{i=r+1}^{d_M} c_i,$$

where c_i is the i^{th} eigenvalue of the covariance C . Moreover, it is established (by Proposition 3.1 in [70]) that the upper bound of the active subspace projection error in (2.6) is smaller or equal to the upper bound of the KLE projection error in (2.10), i.e.,

$$(2.11) \quad \sum_{i=r+1}^{d_M} \lambda_i^M \leq L^2 \sum_{i=r+1}^{d_M} c_i.$$

Both KLE and AS can be used to detect low dimensionality of the input space, as well as to provide dominant basis vectors for the input space. KLE can be used to reduce the input dimensionality when the covariance of the parameter distribution ν has quick decay. The issue with KLE is that it does not take into account the outputs q . In contrast, AS can be used to reduce the input dimensionality when the covariance preconditioned Gauss-Newton Hessian has quick eigenvalue decay, which directly takes into account the sensitivity of the outputs to the input parameters and can be used in a more broad set of circumstances than KLE. It is likely that the AS projection is more accurate than the KLE projection, informed by the relation of their error bounds (2.11), and demonstrated by our numerical experiments.

The limitations of the AS approach are that the parametric mapping is assumed to be differentiable with respect to the parameters m , and that the computation of the AS basis is formally more expensive than the computation of the KLE basis. Both bases can be calculated via matrix free randomized methods [40], which do not require the explicit formation of the matrices, and instead require only matrix-vector products. KLE requires access to just the covariance operator, while AS require evaluations of the Jacobian of the parametric mapping at different sample points. However, the Jacobian matrix-vector products required in the computation of the AS subspace require only marginally more work than the computation of the training data. This is because once the forward PDE is solved at a sample point to construct a training data pair, the Jacobian matrix-vector product at that point requires solution of linearized forward and adjoint PDE problems with $O(r)$ right hand sides each. When direct (or iterative solvers with expensive-to-construct preconditioners) are employed to solve these problems, little additional work is required beyond the forward solve. This is because triangular solves are asymptotically cheap compared to the factorizations (or for iterative solves, the preconditioner needs to be constructed just once). Moreover, blocking the $O(r)$ right hand sides in the forward/adjoint solves results in better cache performance, thereby making the Jacobian action less expensive that it might seem. In practice AS may require fewer samples than training data construction (in numerical experiments we use significantly fewer samples for AS construction than training data). When the spectrum of the parameter covariance-preconditioned Gauss-Newton Hessian decays rapidly, r is small and only few matrix-vector products (and hence linearized forward/adjoint solves) are required. For more information see Appendix A.

2.2. Output Projection: Proper Orthogonal Decomposition. Reduced order modeling (ROM), e.g. a reduced basis method (RBM) have been developed

to help reduce the dimension of PDE outputs (solution and quantities of interest) [8, 26, 27, 59, 66]. This methodological framework has made tractable the solution of many-query problems involving PDEs (optimization, inference, control, inverse problems etc.) [13]. In these methods low dimensional representations of the outputs are made via snapshots. Due to the optimality of the representation in the sense of Proposition 2.1, this approach is also considered for solving parametric PDEs using dimension reduced neural networks [9].

The proper orthogonal decomposition (POD) for the outputs is the eigenvalue decomposition of the expectation of the following matrix,

$$(2.12) \quad \mathbb{E}_\nu[qq^T] = \int_{\mathbb{R}^{d_M}} q(m)q(m)^T d\nu(m) = \Phi D \Phi^T.$$

Using the Hilbert-Schmidt Theorem, the POD basis is shown to be optimal for the following minimization problem (see [48, 59]).

PROPOSITION 2.1 (Proposition 2.1 in [48]). *The POD basis $\Phi \in \mathbb{R}^{d_Q \times r_Q}$ is such that*

$$(2.13) \quad \int_{\mathbb{R}^{d_M}} \|q(m) - \Phi \Phi^T q(m)\|_{\ell^2(\mathbb{R}^{d_Q})}^2 d\nu(m) \\ = \min_{W \in \mathbb{R}^{d_Q \times r_Q}, W^T W = I_{r_Q}} \int_{\mathbb{R}^{d_M}} \|q(m) - W W^T q(m)\|_{\ell^2(\mathbb{R}^{d_Q})}^2 d\nu(m).$$

And the error is given by the trailing eigenvalues of $\mathbb{E}_\nu[qq^T]$:

$$(2.14) \quad \int_{\mathbb{R}^{d_M}} \|q(m) - \Phi \Phi^T q(m)\|_{\ell^2(\mathbb{R}^{d_Q})}^2 d\nu(m) = \sum_{i=r_Q+1}^{\text{rank}(T)} \lambda_i^Q$$

POD serves as a constructive prescription for a low rank basis that is optimal in the ℓ^2 sense. It also serves as a means of reliably calculating the inherent dimensionality of the outputs for the mapping $m \mapsto q$. The POD basis can be approximated via Monte Carlo samples directly from training data using the “method of snapshots” [58].

2.3. Input–Output Error Bound for Optimal Ridge Function. Reduced bases for the parameter space \mathbb{R}^{d_M} and the output space \mathbb{R}^{d_Q} can be used to design input–output reduced ridge function surrogates for the mapping $m \mapsto q$ as in Equation (2.1). When the input dimensions that inform the outputs are well approximated by the modes spanned by V_{r_M} , and the outputs are well approximated when restricted to the span of Φ_{r_Q} , then the mapping $m \mapsto q$ can be well approximated by ridge functions of this form. A schematic for this ridge function strategy is given in Figure 1.

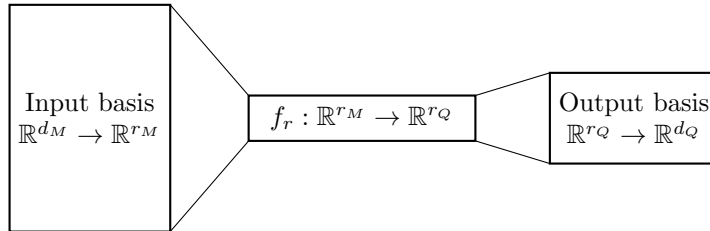


Fig. 1: Dimension reduced representation by conditional expectation ridge function.

Combining each of the KLE and AS approaches with POD, an error bound can be established for the conditional expectation ridge function that is restricted to the dominant modes of the POD basis.

PROPOSITION 2.2 (Input–Output Ridge Function Error Bound).

Let $P_{r_M} = V_r V_r^T C^{-1} \in \mathbb{R}^{d_M}$ be the projectors coming from the active subspace generalized eigenvalue problem (2.5), and define the conditional expectation of the outputs q with respect to the σ -algebra generated P_{r_M} given in Equation (2.7):

$$(2.15) \quad q_{r_M}(m) = \mathbb{E}_\nu[q|\sigma(P_{r_M})](m).$$

Define the rank r_Q POD decomposition for q_{r_M} as follows:

$$(2.16) \quad [\mathbb{E}_\nu[q_{r_M} q_{r_M}^T]]_{r_Q} = \left[\int_{\mathbb{R}^{d_M}} q_{r_M}(m) q_{r_M}(m)^T d\nu(m) \right]_{r_Q} = \widehat{\Phi}_{r_Q} \widehat{D}_{r_Q} \widehat{\Phi}_{r_Q}^T.$$

Then one has

$$(2.17) \quad \int_{\mathbb{R}^{d_M}} \|q(m) - \widehat{\Phi}_{r_Q} \widehat{\Phi}_{r_Q}^T q_{r_M}(m)\|_{\ell^2(\mathbb{R}^{d_Q})}^2 d\nu(m) \leq \sum_{i=r_M+1}^{d_M} \lambda_i^M + \sum_{i=r_Q+1}^{d_Q} \lambda_i^Q$$

Further if q is Lipschitz continuous with constant $L \geq 0$, then

$$(2.18) \quad \int_{\mathbb{R}^{d_M}} \|q(m) - \widehat{\Phi}_{r_Q} \widehat{\Phi}_{r_Q}^T q_{r_M}(m)\|_{\ell^2(\mathbb{R}^{d_Q})}^2 d\nu(m) \leq L^2 \sum_{i=r_M+1}^{d_M} c_i + \sum_{i=r_Q+1}^{d_Q} \lambda_i^Q$$

Proof. This result follows from the triangle inequality

$$(2.19) \quad \int_{\mathbb{R}^{d_M}} \|q(m) - \widehat{\Phi}_{r_Q} \widehat{\Phi}_{r_Q}^T q_{r_M}(m)\|_{\ell^2(\mathbb{R}^{d_Q})}^2 d\nu(m) \leq \int_{\mathbb{R}^{d_M}} \|q(m) - q_{r_M}(m)\|_{\ell^2(\mathbb{R}^{d_Q})}^2 + \|q_{r_M}(m) - \widehat{\Phi}_{r_Q} \widehat{\Phi}_{r_Q}^T q_{r_M}(m)\|_{\ell^2(\mathbb{R}^{d_Q})}^2 d\nu(m),$$

and application of (2.6),(2.11) and Proposition 2.1. \square

This result establishes that when the spectra for $\mathbb{E}_\nu[\nabla q^T \nabla q]$ and $\mathbb{E}_\nu[qq^T]$ decay rapidly, the map $m \mapsto q$ can be well approximated over ν when restricted to the dominant subspaces of AS and POD. Further if q is Lipschitz continuous with constant L not too large, and the covariance of ν has quick eigenvalue decay, then the map can be well approximated when restricted to the dominant subspace of KLE and POD.

If the mapping $m \mapsto q$ satisfy these conditions, then we just need to find a low dimensional ridge function mapping $f_r : \mathbb{R}^{r_M} \rightarrow \mathbb{R}^{r_Q}$. In the next section we consider feedforward neural networks for the nonlinear ridge functions. This input–output dimension reduction strategy is general and can be readily extended to different nonlinear representations such as polynomials, Gaussian process etc.

3. Projected Neural Network. In this section we present strategies for constructing projecting neural networks. A projected neural network, parametrized by weights $\mathbf{w} = [w, b_Q] \in \mathbb{R}^{d_W}$, can be written as follows:

$$(3.1) \quad f(m, \mathbf{w}) = \Phi_{r_Q} f_r(V_{r_M}^T m, w) + b_Q.$$

The function f_r represents a sequence of nonlinear compositions of affine mappings between successive latent representation spaces $\mathbb{R}^{d_{\text{layer}}}$. The architecture of

the neural network includes the choice of layers, layer dimensions (widths) and non-linear activation functions; for more information see [39]. Once an architecture is chosen, optimal weights are found via the solution of an empirical risk minimization problem over given training data. Here we consider least squares regression: given $\{(m_i, q_i) | m_i \sim \nu\}_{i=1}^{N_{\text{train}}}$, find the weights \mathbf{w} that minimize

$$(3.2) \quad \min_{\mathbf{w} \in \mathbb{R}^{d_W}} \frac{1}{N_{\text{train}}} \sum_{i=1}^{N_{\text{train}}} \|f(m_i, \mathbf{w}) - q(m_i)\|_{\ell^2(\mathbb{R}^{d_Q})}^2.$$

In the setting we consider, a limited number of data are expected to be available for the empirical risk minimization problem. A general rule of thumb is to have a number independent training data N_{train} that is commensurate to the number of weights, d_W , to be inferred, (for linear problems $N_{\text{train}} > d_W/d_Q$ linearly independent data are needed). Since we cannot afford many training data, instead we try to keep d_W small, and the network parsimonious.

A common dimension reduction strategy for regression problems in machine learning is to use an encoder-decoder network [44]. In an encoder-decoder input data is nonlinearly contracted to lower dimensions and then extended to the outputs. The main issue in designing an encoder-decoder is to find a reduced dimensionality that is appropriate. In this setting the intrinsic dimensionalities of the inputs and outputs are exposed by AS, KLE and POD. These decompositions can be used to help identify appropriate dimensions for encoder-decoder architectures.

Additionally the basis representations that result from these decompositions can be used explicitly in the neural network configuration. When training a full neural network (i.e. including the first and last layers as weights) the projectors can be used as initial guesses for neural network training, which can ease the difficulty of the optimization problem, by initializing the portions of the weights corresponding to the first and last layers to regions of the parameter space and outputs that are informed by the parameters m or the parameter-to-output map.

Otherwise one can architect a parsimonious network by keeping the input or output projectors fixed. In this case the dimension of the trainable neural network does not depend explicitly on d_M or d_Q , but only on r_M and r_Q . The network is constrained to only learn patterns between the dominant subspaces of the parameter space and outputs, as exposed by the projectors. If the dependence of the weight dimension on d_M or d_Q is removed by constraining the neural network to the dominant subspaces of the parameter space and outputs, the weights for the neural network can be inferred using few training data. This makes this strategy attractive in settings where the input or output dimensions are very large and the mapping needs to be queried many times, as in many many-query applications including inverse problems, optimal experimental design, forward uncertainty quantification, and optimal control and design.

3.1. Discussion of Errors. In Section 2.3 we discussed errors in approximating $m \mapsto q$ by a ridge function restricted to the dominant modes of both the inputs and outputs. The bounds there are for projection errors. When we attempt to represent the map by a neural network ridge function other errors are introduced. There is an error in the approximation of the low dimensional mapping by the neural network instead of other nonlinear ridge functions. We can think of this error as

$$(3.3) \quad \int_{\mathbb{R}^{d_M}} \|f(m, \mathbf{w}) - q_{r_M}(m)\|_{\ell^2(\mathbb{R}^{d_Q})}^2 d\nu(m) = \text{Representation Error}.$$

Some theoretical guarantees have been established for neural network representation errors; see for example [62, 47, 46]. As was discussed in the previous section, the neural network weights are found via the solution of an empirical risk minimization problem, for which we use Monte Carlo samples to approximate the integral with respect to the parameter distribution ν , which incurs a sampling error that leads to a generalization gap [46]. The empirical risk minimization problem is nonconvex, and so finding a global minimizer is NP-hard. One has to instead settle for local minimizers that perform reasonably well, and this introduces an additional optimization error:

$$(3.4a) \quad \mathbf{w}^\dagger \neq \mathbf{w}^* = \operatorname{argmin} \frac{1}{N_{\text{train}}} \sum_{i=1}^{N_{\text{train}}} \|f(m_i, \mathbf{w}) - q(m_i)\|_{\ell^2(\mathbb{R}^{d_Q})}^2.$$

The approximate solution (\mathbf{w}^\dagger) to the nonconvex optimization problem, is generally different than the global minimizer (\mathbf{w}^*), and the difference between the local minimum and the global minimum is the optimization error

$$(3.4b) \quad \left| \frac{1}{N_{\text{train}}} \sum_{i=1}^{N_{\text{train}}} \|f(m_i, \mathbf{w}^\dagger) - q(m_i)\|_{\ell^2(\mathbb{R}^{d_Q})}^2 - \|f(m_i, \mathbf{w}^*) - q(m_i)\|_{\ell^2(\mathbb{R}^{d_Q})}^2 \right| = \text{Optimization Error}.$$

Recent work suggests that for feedforward neural networks this error can be mitigated by an iterative layerwise optimization procedure [20]. An additional sampling error is incurred in the Monte Carlo approximations made for the computation of the AS and POD projectors. Bounds for such errors are investigated in [42]. In total, the errors incurred can be decomposed into projection error, representation error, sampling errors and optimization error. Each of these errors plays a role in the final solution one gets when constructing a surrogate of this form.

4. Numerical Experiments. We conduct numerical experiments on input-output projection based neural networks on two PDE based regression problems. We consider derivative informed projected neural networks (DIPNets) which use AS for input projection and POD for output projection, we compare this strategy against KLE for input projection and POD for the output projection. Proposition 2.2 suggests that the decay of the eigenvalues for KLE, AS and POD can be used to choose the ranks for these architectures. In order to have a consistent error tolerance criterion between AS and KLE, the Lipschitz constant L appearing in the upper bound (2.11) must be used for comparison. Since this constant is not known a priori, we use fixed ranks in order to have a fair comparison between DIPNet and KLE-to-POD. For simplicity we take the input and output ranks to be the same to demonstrate the generalization accuracy of the projected neural networks compared to the full space network. More representative projected architectures could be achieved by more detailed rank selection procedures, but at additional computational cost.

To demonstrate the benefit of using the projection basis vectors to construct the neural networks, we also use Gaussian random vectors for comparison. Moreover, to demonstrate the projection errors separately, without involving the neural network representation and optimization errors, we also consider the following projection error

$$(4.1) \quad \mathbb{E}_{m \sim \nu} \left[\frac{\|P_{\text{POD}} q(P_{\text{input}} m) - q(m)\|_{\ell^2(\mathbb{R}^{d_Q})}}{\|q(m)\|_{\ell^2(\mathbb{R}^{d_Q})}} \right].$$

Here P_{POD} is the projector on to the principal subspace for the outputs as represented by POD, and P_{input} is the input projector (either AS or KLE). These errors are studied as a function of rank.

For the training of the projected neural network, once the architectures (including projection bases, network layers, layer dimensions, and nonlinear activation functions) are chosen, the locally optimal weights $\mathbf{w}^\dagger \in \mathbb{R}^{d_w}$ are found via solving an empirical risk minimization problem. Given training data $X_{\text{train}} = \{(m_i, q(m_i))\}_{i=1}^{N_{\text{train}}}$, candidate optimal weights are found via solving the empirical risk least-squares minimization problem,

$$(4.2) \quad \min_{w \in \mathbb{R}^{d_w}} F_{X_{\text{test}}}(w) = \frac{1}{2N_{\text{train}}} \sum_{i=1}^{N_{\text{train}}} \|q(m_i) - f(m_i, \mathbf{w})\|_{\ell^2(\mathbb{R}^{d_Q})}^2.$$

We used a subsampled inexact Newton CG method because it performed reliably better than Adam, SGD, and other first order methods on the problems we tested [53]. We define the relative error as

$$(4.3) \quad \text{Relative Error} = \sqrt{\frac{\sum_{i=1}^{N_{\text{test}}} \|q(m_i) - f(m_i, \mathbf{w}^\dagger)\|^2}{\sum_{i=1}^{N_{\text{test}}} \|q(m_i)\|^2}},$$

and the accuracy as

$$(4.4) \quad \text{Accuracy} = 100(1 - \text{Relative Error}).$$

We are particularly interested in what surrogates can achieve good performance with only a limited number of training data, as these are the conditions of the problems that motivate this work. We study the performance of the neural networks as a function of training data, N_{train} . For each problem 2048 total data are generated, with 512 set aside as testing data.

Since the performance of the stochastic optimizer can be sensitive to the choice of initial guesses for the weights not given by the projectors, we average results over ten initial guesses for each neural network, and report averages and standard deviations. We are interested in neural networks that are robust to the choice of initial guess for the weights.

We compare the projected neural networks against a full space neural network. The full space neural network (FS) maps the input data to the output dimension, d_Q . We consider $d_Q < d_M$, so that the FS is not too high dimensional. For both the projected and full space networks we use two nonlinear layers for simplicity and ease of training, with softplus activation functions; these choices performed well during training. For each of the projected neural networks the weights in the input layer are fixed during training, while the weights in the output layer are trained, which we find improved the generalization accuracy. This allows for a neural network with a parsimonious training weight dimension independent of d_M . We do not include the effect of training the input layer in these results; these networks only performed well when the trained input reduced network weights were used as an initial guess, and even then they did not outperform the input reduced networks. This came at the expense of increasing the neural network weight dimension by orders of magnitude. The input and output projectors were orthogonalized and rescaled, which significantly improved generalization accuracy. For more details see Appendix B.1.

The naming conventions we use for the neural networks is “DIPNet” for the neural networks that use the AS projector for the input and the POD projector for the outputs. We call the networks that use KLE for the input and POD for the output “KLE” networks. We call the Gaussian random projected networks “RS” for random space, and the full space networks “FS.” We investigate two numerical examples that involve parametric maps related to PDE-governed inference problems.

The first example is a 2D semi-linear convection-diffusion-reaction PDE, where the parameters m represents a coefficient in a nonlinear reaction term. The second example is a 2D Helmholtz PDE with a single source, where the parameters m represents a variable coefficient. In both examples the outputs are the PDE state evaluated at some points the interior of the PDE domain.

Both problems use a Gaussian distribution with Matérn covariance for the uncertain parameter distribution $\nu(m)$, for more information see Appendix B.2. The Matérn covariance can be represented by the inverse of a coercive elliptic operator. The KLE basis vectors are taken as eigenvectors corresponding to the leading eigenvalues of the discrete covariance, discretized by a finite element method.

4.1. Convection-Diffusion-Reaction Problem. For a first case study, we investigate a 2D quasi-linear convection-diffusion-reaction problem with a nonlinear reaction term. The formulation of the problem is

$$\begin{aligned}
 (4.5a) \quad & -\nabla \cdot (k\nabla u) + \mathbf{v} \cdot \nabla u + e^m u^3 = f \quad \text{in } \Omega \\
 (4.5b) \quad & u = 0 \quad \text{on } \partial\Omega \\
 (4.5c) \quad & q(m) = Bu(m) = [u(\mathbf{x}^{(i)}, m)] \quad \text{at } \mathbf{x}^{(i)} \in (0.6, 0.8)^2 \\
 (4.5d) \quad & \Omega = (0, 1)^2.
 \end{aligned}$$

where m is a mean-zero random field representing the log-coefficient of the reaction term. The volumetric forcing function f is a Gaussian bump located at $x_1 = 0.7, x_2 = 0.7$. The velocity field \mathbf{v} used for each simulation is the solution of a steady-state Navier-Stokes equation with side walls driving the flow. See Appendix B for more information.

Here we consider unit square meshes parametrized by n_x, n_y . We study two meshes, $n_x = n_y = 64$ and $n_x = n_y = 192$. The Gaussian Matérn distribution for ν is parametrized by $\gamma = 0.1, \delta = 1.0$. We start by investigating the eigenvalue decompositions for AS, KLE and POD, and the input-output projection errors given by 4.1.

In Figure 2, the AS spectra agree between the two mesh discretization and are roughly mesh independent. The KLE spectra agree between the two mesh discretization and are roughly mesh independent. The decay of the AS spectra are quicker than those of the KLE spectra.

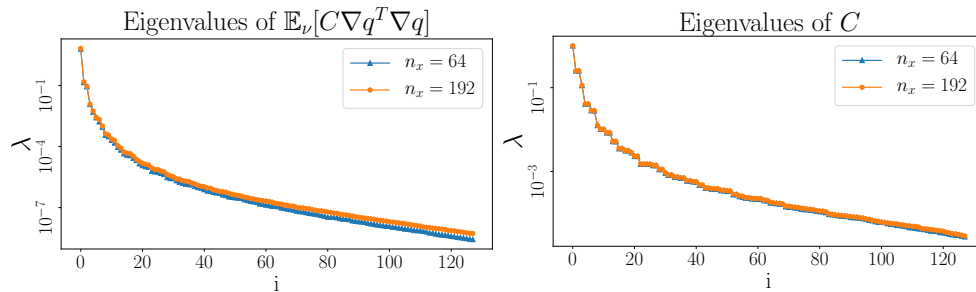


Fig. 2: Active subspace and KLE eigenvalue decay for $\gamma = 0.1, \delta = 1.0$

In Figure 3, the dominant vectors of AS are localized to the part of the domain where the observations are present. The KLE eigenvectors represent the dominant eigenmodes of the fractional PDE operator that is the covariance matrix. For this problem, which has Dirichlet boundary conditions and a unit square mesh, these modes correspond to the constant, and sines and cosines that arise in separation of variables. These eigenvectors do not pick up local information about the mapping $m \mapsto q$.

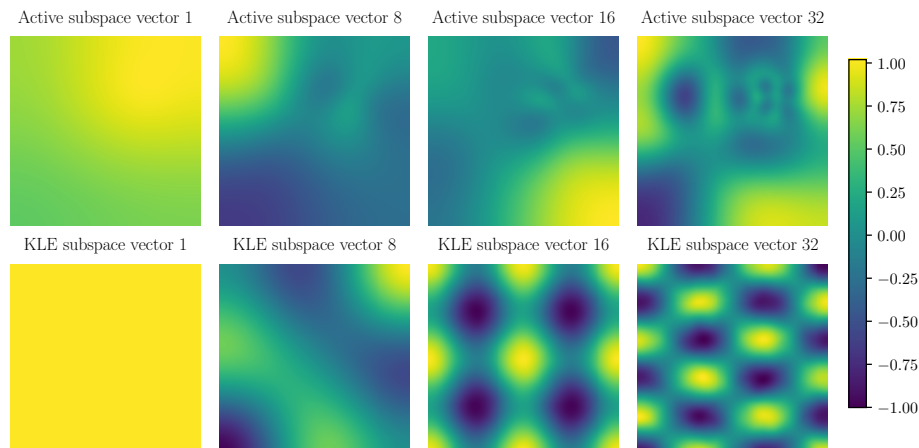


Fig. 3: AS and KLE eigenvectors for $\gamma = 0.1, \delta = 1.0$

In Figure 4, the POD spectra agree in the dominant modes and have similar qualitative decay. They however begin to diverge in the small modes, the finer discretization contains more information in the tail of the spectrum. The input–output error projection errors in Figure 4 are sample average approximations of equation 4.1 computed for AS and KLE. Both use POD for the outputs, and in each case the ranks are taken to be the same for both the input and the output projectors. Since the output projectors are taken to be the same, this allows for a study of how informed the input projectors are. The AS projector contains more information that informs the outputs than KLE, particularly in the first 15 – 20 modes, after that the decay rate of the projection errors are roughly the same.

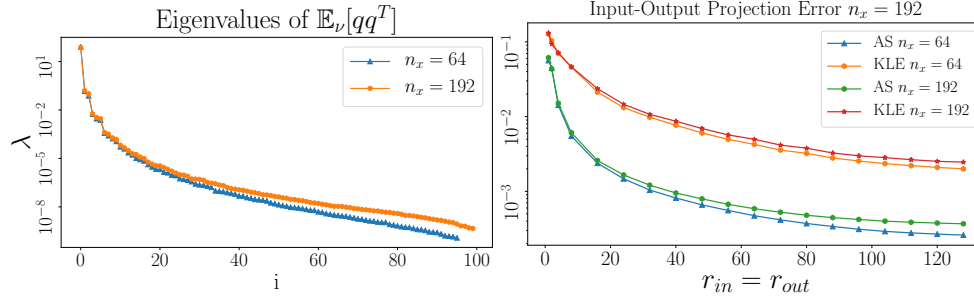


Fig. 4: Plot of spectra for POD on the two meshes (left), and the input–output projection error (right) for the convection-diffusion-reaction problem

In what follows we train the projected neural networks and compare against the FS network. Below in Table 1, dimensions for the input parameters d_M , and neural network weight dimension d_W for each network are summarized.

d_M	4, 225	37, 249
(DIPNet, KLE, RS) projected network $r = 8$	1, 124	1, 124
(DIPNet, KLE, RS) projected network $r = 32$	6, 500	6, 500
(DIPNet, KLE, RS) projected network $r = 128$	49, 740	49, 740
FS network	442, 800	3, 745, 200

Table 1: Neural network weight dimensions and parameter dimension for different meshes.

For a first set of results we compare the rank $r = 8$ projected networks with the FS network for the coarse mesh. In Figure 5, the DIPNet performs better than all three other networks. The KLE network performs about 2% worse in generalization accuracy, both of these networks perform about the same for different initial guesses for the inner dense layer weights. The RS network performs better than the FS network, which suggests that the reduced dimension architecture has benefits in this regime, however it is very sensitive to the initial guesses for the weights as indicated by the one standard deviation error bars. The DIPNet and KLE networks perform significantly better than the RS network which suggests that there is definite upside to choosing input and output bases for these networks.

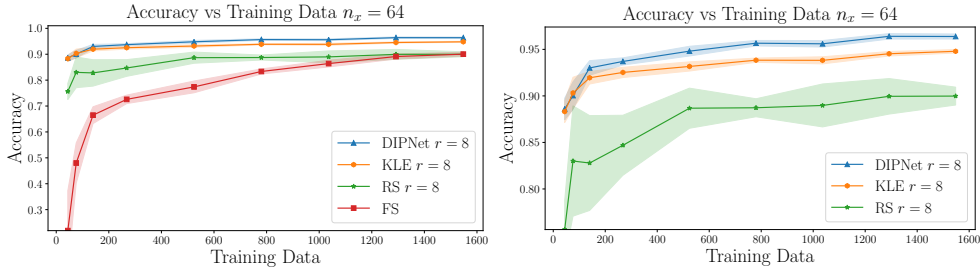


Fig. 5: Generalization accuracy vs number of training data seen for all networks (left), and just the projected networks (right) for the coarse mesh convection-diffusion-reaction problem.

Figure 6 shows that as the parameter dimension d_M grows, the RS and FS networks become harder to train, while the DIPNet and KLE networks perform comparably well to how they did for the coarse mesh. This suggests that there is mesh independent information that can be encapsulated by the AS, KLE and POD eigenvectors.

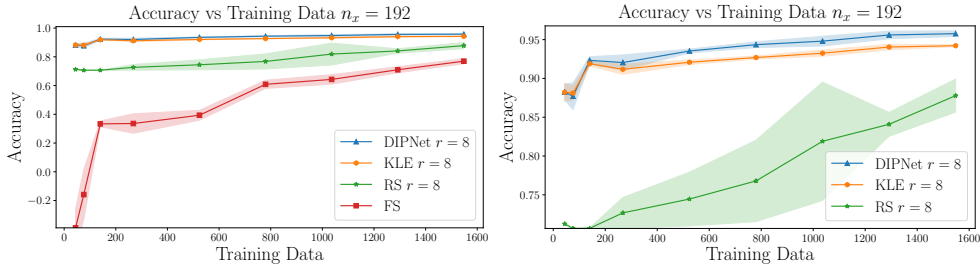


Fig. 6: Accuracy vs number of training data seen for all networks (left), and just the projected networks (right) for the fine mesh convection-diffusion-reaction problem.

For the next set of numerical results we compare the performance of the DIPNet and KLE projected networks for different choices of the rank r . Figure 7 shows that the advantages of the DIPNet are pronounced when the rank is small, but as the rank r grows the KLE network starts to catch up. While the superior performance of DIPNet in low dimensions agrees with the projection errors observed in Figure 4, the comparable performance of KLE to DIPNet for higher dimensions does not agree. We believe that this has to do with the errors inherent in the neural network representation and training, as discussed in Section 3.1.

As the input bases grow, there will be more overlap between AS and KLE, and more room for the KLE network to learn patterns captured by the low dimensional AS basis. Note also that generally, as the input and output bases grow, the variance with respect to the neural network initial guesses decreases. Similar trends are observed in Figure 8 for the finer mesh discretization.

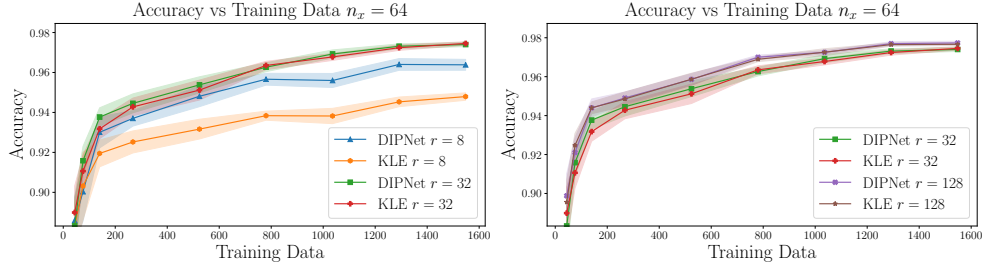


Fig. 7: Accuracy vs number of training data seen for DIPNet and KLE networks as a function of rank for the coarse mesh convection-diffusion-reaction problem.

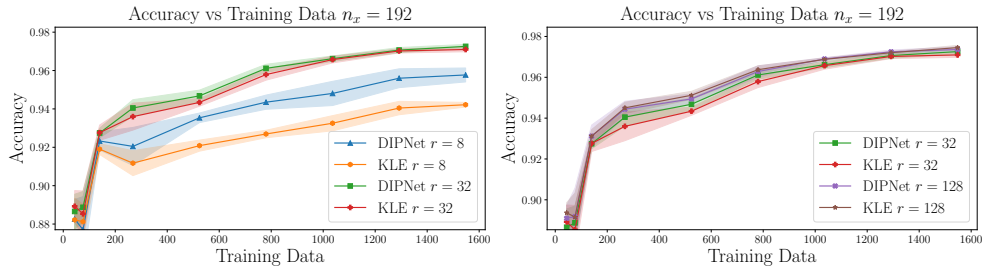


Fig. 8: Accuracy vs number of training data seen for DIPNet and KLE networks as a function of rank for the fine mesh convection diffusion problem.

4.2. Helmholtz Problem. For a second case study, we investigate a 2D Helmholtz problem with a nonlinear dependence on the random field m , which represents the log-prefactor of the wavenumber k . The formulation of the problem is

$$(4.6a) \quad -\Delta u - (ke^m)^2 u = f \quad \text{in } \Omega$$

$$(4.6b) \quad \text{PML boundary condition on } \partial\Omega \setminus \Gamma_{\text{top}}$$

$$(4.6c) \quad \nabla u \cdot n = 0 \quad \text{on } \Gamma_{\text{top}}$$

$$(4.6d) \quad q(m) = Bu(m) = [u(\mathbf{x}^{(i)}, m)] \quad \text{at } \mathbf{x}^{(i)} \in \Omega$$

$$(4.6e) \quad \Omega = (0, 3)^2.$$

The PML boundary condition on the sides and bottom of the domain simulates truncation of a semi-infinite domain; waves can only be reflected on the top surface. Due to the PML domain truncation, the PDE for the Matérn covariance for the parameter distribution has Robin boundary conditions to eliminate boundary artifacts [36]. The problem has a single source at a point $(0.775, 2.85)$, and the 100 observation points are clustered in a box $(0.575, 0.975) \times (2.75, 2.95)$, none of the observation points coincide with the source. Since the PDE state variable here is a velocity field, the outputs have dimension $d_Q = 200$ for this problem. The wave number for this problem is 9.118. The Gaussian Matérn distribution ν is parametrized by $\gamma = 1.0, \delta = 5.0$. We consider two meshes for this problem again, $n_x = n_y = 64$ and 128. We again

start by investigating the eigenvalue decompositions for AS, KLE and POD, and the input–output projection errors given by 4.1.

In Figure 9, the AS spectra agree between the two mesh discretization and are roughly mesh independent. Note that for this problem the decay of the dominant modes of the AS spectra compared to KLE are much more pronounced than in Figure 2. The KLE spectra agree between the two mesh discretization and are roughly mesh independent.

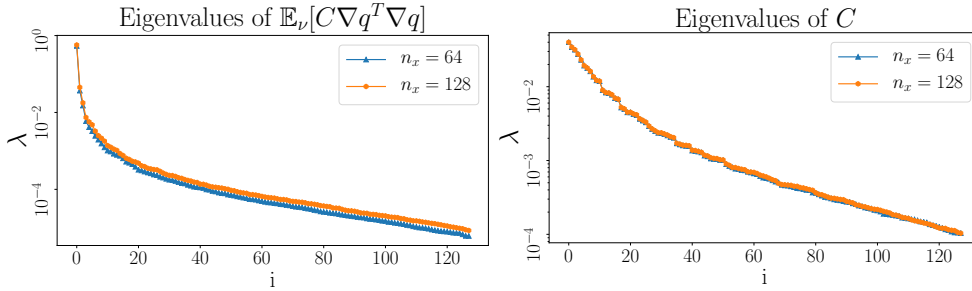


Fig. 9: Active subspace and KLE spectra for $\gamma = 1.0, \delta = 5.0$

The dominant AS vectors are localized to the part of the domain where the observations are present. The first mode captures strictly locally supported information of the uncertain parameters, and the higher modes start to capture higher frequency effects inherent to the Helmholtz problem. The KLE eigenvectors again correspond to the eigenvectors arising from separation of variables, note that for this problem the PDE forward map is dissimilar to the covariance operator, so this basis is not an optimal representation of the PDE state, and therefore a linear restriction of the PDE state. These eigenvectors again do not pick up local information about the mapping $m \mapsto q$.

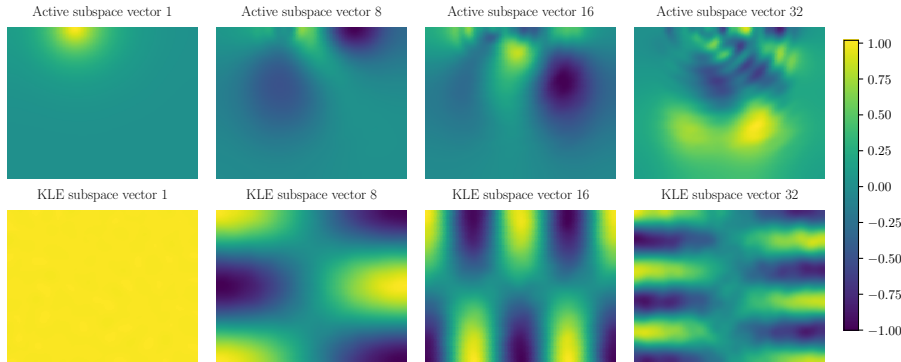


Fig. 10: AS and KLE eigenvectors for $\gamma = 1.0, \delta = 5.0$

In Figure 11, the POD spectra agree in the dominant modes and have similar qualitative decay. They however begin to diverge in the small modes—even more so than in the convection-diffusion-reaction problem. The finer discretization contains

more information in the tail of the spectrum. The AS projector contains more information about the outputs than KLE, particularly in the first 15 – 20 modes, after that the decay rate of the projection errors are roughly the same.

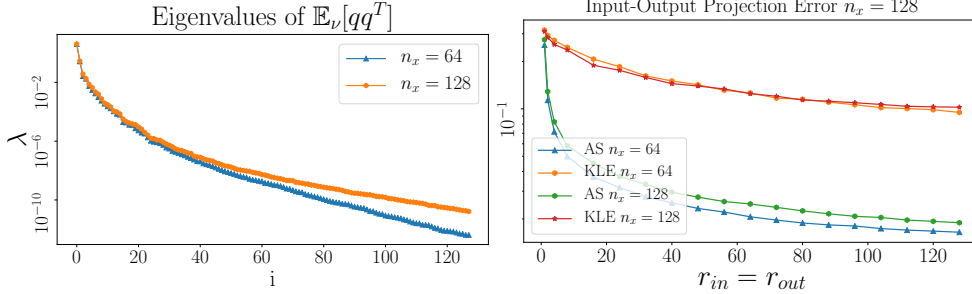


Fig. 11: Plot of spectra for POD on the two meshes (left), and the input–output projection error (right) for the Helmholtz problem

In what follows we train the projected neural network networks and compare against the FS networks. Below in Table 2, dimensions for the input parameters d_M , and d_W for each network are summarized.

d_M	4, 225	16, 641
(DIPNet, KLE, RS) projected network $r = 8$	2, 024	2, 024
(DIPNet, KLE, RS) projected network $r = 32$	9, 800	9, 800
(DIPNet, KLE, RS) projected network $r = 64$	25, 544	25, 544
FS network	925, 600	3, 408, 800

Table 2: Neural network weight dimensions and parameter dimension for the different meshes used.

For a first set of results we again compare the rank $r = 8$ projected networks with the FS network for the coarse mesh. In Figure 12, the DIPNet performs better than all three other networks. For this problem the KLE network performs about 10% worse in generalization accuracy, both of these networks perform about the same for different initial guesses for the inner dense layer weights. The RS and KLE networks performs better than the FS network in the low data regime, but the FS network begins to outperform these two networks when more training data are available. The FS network nearly catches up to the DIPNet $r = 8$ network in the high data limit. The benefit of the DIPNet and FS networks over the KLE and RS networks seems to be their ability to resolve more oscillatory information than the KLE and RS networks. The FS network is able to do this when more data are available, since it has many weights to be fit, the DIPNet can do this in both the limited data regime and when more data are available, since the AS basis is able to represent these modes. The KLE network represents smooth modes of the parameter distribution covariance, which are not as useful when the parametric mapping is dominated by highly oscillatory modes as in this example.

The benefit of KLE for the convection-diffusion-reaction problem is that the PDE

problem was similar to the PDE that shows up in the Gaussian Matérn covariance matrix. The limitations of KLE show up for the Helmholtz problem, where the forward PDE mapping is dissimilar from the parameter distribution covariance operator C .

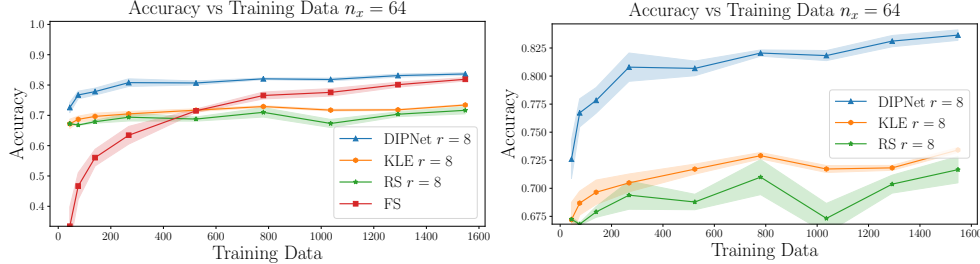


Fig. 12: Accuracy vs number of training data seen for all networks (left), and just the projected networks (right) for the coarse mesh Helmholtz problem.

Figure 13 shows that as the parameter dimension d_M grows, the RS and FS networks become harder to train, while the DIPNet and KLE networks perform comparably well to how they did for the coarse mesh. The FS network again nearly catches up the the DIPNet $r = 8$ in the high data limit.

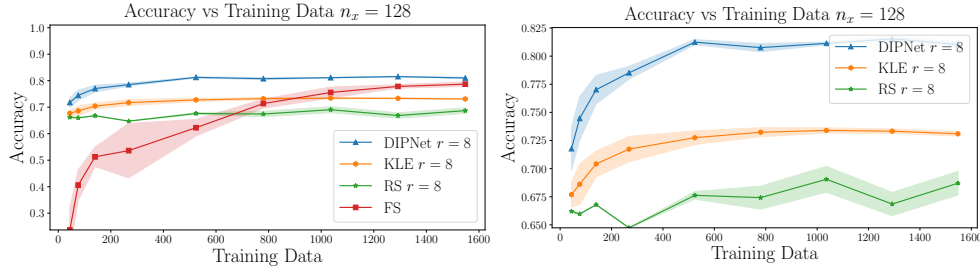


Fig. 13: Accuracy vs number of training data seen for all networks (left), and just the projected networks (right) for the fine mesh Helmholtz problem.

For the next set of numerical results we again compare the performance of the DIPNet and KLE projected networks for different choices of the rank r . Figure 14 shows that for this problem the DIPNet outperforms the KLE networks consistently. The low dimensional ($r = 8$) DIPNet performs well for low data, but sees reduced performance as the data dimension improves. The DIPNets see benefited performance when the rank increases to 32 and 64. Both KLE and DIPNet observed reduced accuracy for $r = 128$. The Helmholtz data are evidently harder to fit than the convection-diffusion-reaction data, which are less oscillatory as seen by the AS eigenvectors for the two problems (Figures 3 and 10). When the dimension of the neural networks grow sufficiently large the difficulties of neural network training begin to dominate the benefits of better approximation in larger reduced bases.

Similar trends are observed in Figure 15.

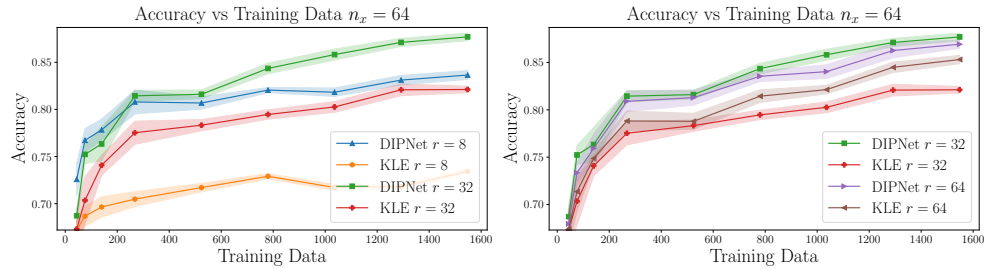


Fig. 14: Accuracy vs number of training data seen for DIPNet and KLE networks as a function of rank for the coarse mesh Helmholtz problem.

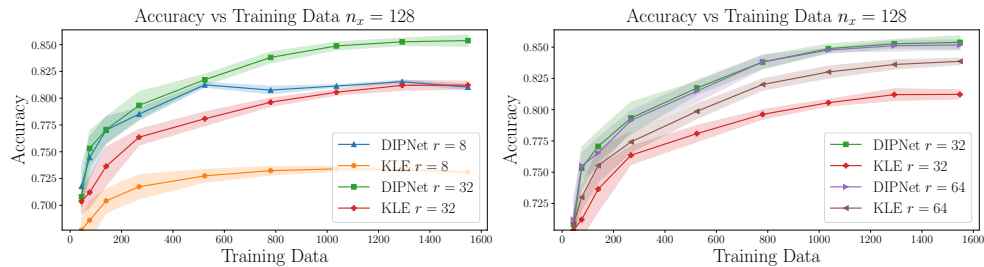


Fig. 15: Accuracy vs number of training data seen for DIPNet and KLE networks as a function of rank for the fine mesh Helmholtz problem.

In these numerical results we compared fixed ranks for the inputs and the outputs, in order to have a straightforward comparison between the DIPNet and KLE networks. In general we recommend the use of the DIPNet, which uses explicit information of the parametric map to construct an informed subspace of the input. The decay of the AS and POD spectra alone can be used to decide the ranks of the input and output projectors for the networks, with the projection error result from Proposition 2.2 in mind for this rank choice. This result is less useful when using the KLE spectral decay in choosing a network structure, since this additionally requires knowledge of the Lipschitz constant L for the mapping $m \mapsto q$. Further, numerical results demonstrate that when the PDE mapping does not look like the covariance operator, KLE does not perform much better than random projectors, while the DIPNet performed well for both numerical experiments.

4.3. Software. Code for the numerical experiments can be found in hIPPYflow[55], a Python library for parametric PDE based dimension reduction and surrogate modeling based on hIPPYlib[64, 65], a Python library for adjoint based inference problems. Neural network training was carried out by hessianlearn[52], a Python library for Hessian based stochastic optimization in TensorFlow and Keras [1, 53, 54].

5. Conclusions. In this work we have presented a framework for the dimension-independent construction of derivative-informed projected neural network (DIPNet) surrogates for parametric maps governed by partial differential equations. The need

for these surrogates arises in many-query problems for expensive-to-solve PDEs characterized by high-dimensional parameters. Such settings are challenging for surrogate construction, since the expense of the PDE solves implies that a limited number of data can be generated for training, far fewer than typical data-hungry surrogates require in high dimensions. In order to address these challenges, we present projected neural networks that use derivative (Jacobian) information for input dimension reduction and principal subspaces of the output to construct parsimonious networks architectures. We advocate the use of Jacobian-informed active subspace (AS) projection for the parameters, and proper orthogonal decomposition (POD) projection for the outputs, and motivate the strategy with analysis.

In numerical experiments we compare this DIPNet strategy against a similar strategy that instead uses Karhunen Loève Expansion (KLE) for the input dimension [9], conventional full space dense networks, and similarly architected projected neural networks using random projectors for the input and output bases. The full space network performed poorly in the low data regime, demonstrating the need for projected neural networks in high dimensional surrogate problems with few training data. The DIPNet and KLE-to-POD networks outperformed the random subspace projected network, showing that it is important to choose basis vectors for the input and output representation in the neural network that exploit the structure of the parametric PDE-based map.

The KLE-to-POD strategy worked well for the convection-diffusion-reaction problem, but not as well for the Helmholtz problem. On the other hand, the DIPNet strategy performed well in both numerical examples, consistently outperforming all of the other neural networks. This makes sense in light of the projection error plots (Figure 4 and Figure 11); in the convection-diffusion-reaction case the KLE basis was able to reduce the error similar to AS, but in the Helmholtz case the KLE basis was unable to reduce the projection error to any significant degree. Figures 3 and 10 demonstrate that in both cases the AS eigenvectors were able to resolve key localized information, in particular highly-oscillatory smaller length scales for the Helmholtz problem, while the KLE eigenvectors resembled typical elliptic PDE eigenfunctions as expected.

These projectors used in DIPNet are infinite-dimensionally consistent, meaning that the neural network learns the true information for the PDE and not artifacts of the discretization. This strategy allows for extensions to transfer learning and multi-fidelity methods.

In future work we will employ these surrogates in many-query settings such as Bayesian inference, optimal experimental design, and stochastic optimization. The neural network architectures in this work were kept simple in order to limit the sources of errors (more complicated neural networks are harder to train). There is considerable opportunity to tune the parametrizations of the input–output projected networks to achieve higher performing networks. Nevertheless, the present work demonstrates the power of our general approach.

REFERENCES

- [1] M. ABADI, A. AGARWAL, P. BARHAM, E. BREVDO, Z. CHEN, C. CITRO, G. S. CORRADO, A. DAVIS, J. DEAN, M. DEVIN, ET AL., *TensorFlow: Large-scale machine learning on heterogeneous distributed systems*, arXiv preprint arXiv:1603.04467, (2016).
- [2] A. ALEXANDERIAN, N. PETRA, G. STADLER, AND O. GHATTAS, *A-optimal design of experiments for infinite-dimensional Bayesian linear inverse problems with regularized ℓ_0 -sparsification*, *SIAM Journal on Scientific Computing*, 36 (2014), pp. A2122–A2148, <https://doi.org/10.1137/130933381>.

- [3] A. ALEXANDERIAN, N. PETRA, G. STADLER, AND O. GHATTAS, *A fast and scalable method for A-optimal design of experiments for infinite-dimensional Bayesian nonlinear inverse problems*, SIAM Journal on Scientific Computing, 38 (2016), pp. A243–A272, <https://doi.org/10.1137/140992564>.
- [4] A. ALEXANDERIAN, N. PETRA, G. STADLER, AND O. GHATTAS, *Mean-variance risk-averse optimal control of systems governed by PDEs with random parameter fields using quadratic approximations*, SIAM/ASA Journal on Uncertainty Quantification, 5 (2017), pp. 1166–1192, <https://doi.org/10.1137/16M106306X>. arXiv preprint arXiv:1602.07592.
- [5] N. ALGER, P. CHEN, AND O. GHATTAS, *Tensor train construction from tensor actions, with application to compression of large high order derivative tensors*, SIAM Journal on Scientific Computing, 42 (2020), pp. A3516–A3539.
- [6] I. BABUŠKA, F. NOBILE, AND R. TEMPONE, *A stochastic collocation method for elliptic partial differential equations with random input data*, SIAM review, 52 (2010), pp. 317–355.
- [7] O. BASHIR, K. WILLCOX, O. GHATTAS, B. VAN BLOEMEN WAANDERS, AND J. HILL, *Hessian-based model reduction for large-scale systems with initial condition inputs*, International Journal for Numerical Methods in Engineering, 73 (2008), pp. 844–868.
- [8] P. BENNER, S. GUGERCIN, AND K. WILLCOX, *A survey of projection-based model reduction methods for parametric dynamical systems*, SIAM review, 57 (2015), pp. 483–531.
- [9] K. BHATTACHARYA, B. HOSSEINI, N. B. KOVACHKI, AND A. M. STUART, *Model reduction and neural networks for parametric pdes*, arXiv preprint arXiv:2005.03180, (2020).
- [10] J. BRANKE, *Evolutionary algorithms for neural network design and training*, Citeseer, 1995.
- [11] M. M. BRONSTEIN, J. BRUNA, Y. LECUN, A. SZLAM, AND P. VANDERGHEYNST, *Geometric deep learning: going beyond euclidean data*, IEEE Signal Processing Magazine, 34 (2017), pp. 18–42.
- [12] T. BUI-THANH, C. BURSTEDDE, O. GHATTAS, J. MARTIN, G. STADLER, AND L. C. WILCOX, *Extreme-scale UQ for Bayesian inverse problems governed by PDEs*, in SC12: Proceedings of the International Conference for High Performance Computing, Networking, Storage and Analysis, 2012. Gordon Bell Prize finalist.
- [13] T. BUI-THANH, M. DAMODARAN, AND K. WILLCOX, *Aerodynamic data reconstruction and inverse design using proper orthogonal decomposition*, AIAA journal, 42 (2004), pp. 1505–1516.
- [14] T. BUI-THANH AND O. GHATTAS, *Analysis of the Hessian for inverse scattering problems. Part I: Inverse shape scattering of acoustic waves*, Inverse Problems, 28 (2012), p. 055001, <https://doi.org/10.1088/0266-5611/28/5/055001>.
- [15] T. BUI-THANH AND O. GHATTAS, *Analysis of the Hessian for inverse scattering problems. Part II: Inverse medium scattering of acoustic waves*, Inverse Problems, 28 (2012), p. 055002, <https://doi.org/10.1088/0266-5611/28/5/055002>.
- [16] T. BUI-THANH AND O. GHATTAS, *Analysis of the Hessian for inverse scattering problems. Part III: Inverse medium scattering of electromagnetic waves*, Inverse Problems and Imaging, 7 (2013), pp. 1139–1155.
- [17] T. BUI-THANH AND O. GHATTAS, *A scalable MAP solver for Bayesian inverse problems with Besov priors*, Inverse Problems and Imaging, 9 (2015), pp. 27–54.
- [18] T. BUI-THANH, O. GHATTAS, J. MARTIN, AND G. STADLER, *A computational framework for infinite-dimensional Bayesian inverse problems Part I: The linearized case, with application to global seismic inversion*, SIAM Journal on Scientific Computing, 35 (2013), pp. A2494–A2523, <https://doi.org/10.1137/12089586X>.
- [19] T. BUI-THANH, K. WILLCOX, AND O. GHATTAS, *Model reduction for large-scale systems with high-dimensional parametric input space*, SIAM Journal on Scientific Computing, 30 (2008), pp. 3270–3288.
- [20] K. H. R. CHAN, Y. YU, C. YOU, H. QI, J. WRIGHT, AND Y. MA, *Deep networks from the principle of rate reduction*, arXiv preprint arXiv:2010.14765, (2020).
- [21] P. CHEN AND O. GHATTAS, *Hessian-based sampling for high-dimensional model reduction*, International Journal for Uncertainty Quantification, 9 (2019).
- [22] P. CHEN AND O. GHATTAS, *Projected Stein variational gradient descent*, in Advances in Neural Information Processing Systems, 2020.
- [23] P. CHEN AND O. GHATTAS, *Taylor approximation for chance constrained optimization problems governed by partial differential equations with high-dimensional random parameters*, arXiv preprint arXiv:2011.09985, (2020).
- [24] P. CHEN, M. HABERMAN, AND O. GHATTAS, *Optimal design of acoustic metamaterial cloaks under uncertainty*, Journal of Computational Physics, 431 (2021), p. 110114.
- [25] P. CHEN AND A. QUARTERONI, *A new algorithm for high-dimensional uncertainty quantification based on dimension-adaptive sparse grid approximation and reduced basis methods*, Journal

- of Computational Physics, 298 (2015), pp. 176–193.
- [26] P. CHEN, A. QUARTERONI, AND G. ROZZA, *A weighted reduced basis method for elliptic partial differential equations with random input data*, SIAM Journal on Numerical Analysis, 51 (2013), pp. 3163–3185.
- [27] P. CHEN, A. QUARTERONI, AND G. ROZZA, *Reduced basis methods for uncertainty quantification*, SIAM/ASA Journal on Uncertainty Quantification, 5 (2017), pp. 813–869.
- [28] P. CHEN AND C. SCHWAB, *Model order reduction methods in computational uncertainty quantification*, Handbook of uncertainty quantification, (2016), pp. 1–53.
- [29] P. CHEN, U. VILLA, AND O. GHATTAS, *Hessian-based adaptive sparse quadrature for infinite-dimensional bayesian inverse problems*, Computer Methods in Applied Mechanics and Engineering, 327 (2017), pp. 147–172.
- [30] P. CHEN, U. VILLA, AND O. GHATTAS, *Taylor approximation and variance reduction for PDE-constrained optimal control under uncertainty*, Journal of Computational Physics, 385 (2019), pp. 163–186, <https://arxiv.org/abs/1804.04301>.
- [31] P. CHEN, U. VILLA, AND O. GHATTAS, *Taylor approximation and variance reduction for pde-constrained optimal control under uncertainty*, Journal of Computational Physics, 385 (2019), pp. 163–186.
- [32] P. CHEN, K. WU, J. CHEN, T. O'LEARY-ROSEBERRY, AND O. GHATTAS, *Projected Stein variational Newton: A fast and scalable Bayesian inference method in high dimensions*, Advances in Neural Information Processing Systems, (2019).
- [33] A. COHEN AND R. DEVORE, *Approximation of high-dimensional parametric PDEs*, Acta Numerica, 24 (2015), pp. 1–159.
- [34] P. G. CONSTANTINE, E. DOW, AND Q. WANG, *Active subspace methods in theory and practice: applications to kriging surfaces*, SIAM Journal on Scientific Computing, 36 (2014), pp. A1500–A1524.
- [35] B. CRESTEL, A. ALEXANDERIAN, G. STADLER, AND O. GHATTAS, *A-optimal encoding weights for nonlinear inverse problems, with application to the Helmholtz inverse problem*, Inverse Problems, 33 (2017), p. 074008, <http://iopscience.iop.org/10.1088/1361-6420/aa6d8e>.
- [36] Y. DAON AND G. STADLER, *Mitigating the influence of boundary conditions on covariance operators derived from elliptic PDEs*, Inverse Problems and Imaging, 12 (2018), pp. 1083–1102, <https://arxiv.org/abs/1610.05280>.
- [37] P. H. FLATH, L. C. WILCOX, V. AKÇELİK, J. HILL, B. VAN BLOEMEN WAANDERS, AND O. GHATTAS, *Fast algorithms for Bayesian uncertainty quantification in large-scale linear inverse problems based on low-rank partial Hessian approximations*, SIAM Journal on Scientific Computing, 33 (2011), pp. 407–432, <https://doi.org/10.1137/090780717>.
- [38] I. GARG, P. PANDA, AND K. ROY, *A low effort approach to structured CNN design using PCA*, IEEE Access, (2019).
- [39] I. GOODFELLOW, Y. BENGIO, AND A. COURVILLE, *Deep Learning*, MIT Press, 2016. <http://www.deeplearningbook.org>.
- [40] N. HALKO, P.-G. MARTINSSON, AND J. A. TROPP, *Finding structure with randomness: Probabilistic algorithms for constructing approximate matrix decompositions*, SIAM review, 53 (2011), pp. 217–288.
- [41] J. HAN, A. JENTZEN, AND E. WEINAN, *Solving high-dimensional partial differential equations using deep learning*, Proceedings of the National Academy of Sciences, 115 (2018), pp. 8505–8510.
- [42] J. T. HOLODNAK, I. C. IPSEN, AND R. C. SMITH, *A probabilistic subspace bound with application to active subspaces*, SIAM Journal on Matrix Analysis and Applications, 39 (2018), pp. 1208–1220.
- [43] T. ISAAC, N. PETRA, G. STADLER, AND O. GHATTAS, *Scalable and efficient algorithms for the propagation of uncertainty from data through inference to prediction for large-scale problems, with application to flow of the Antarctic ice sheet*, Journal of Computational Physics, 296 (2015), pp. 348–368, <https://doi.org/10.1016/j.jcp.2015.04.047>.
- [44] M. A. KRAMER, *Nonlinear principal component analysis using autoassociative neural networks*, AIChE journal, 37 (1991), pp. 233–243.
- [45] F. LINDGREN, H. RUE, AND J. LINDSTRÖM, *An explicit link between gaussian fields and gaussian markov random fields: the stochastic partial differential equation approach*, Journal of the Royal Statistical Society: Series B (Statistical Methodology), 73 (2011), pp. 423–498.
- [46] C. MA, S. WOJTOWYTSCH, L. WU, ET AL., *Towards a mathematical understanding of neural network-based machine learning: what we know and what we don't*, arXiv preprint arXiv:2009.10713, (2020).
- [47] C. MA, L. WU, ET AL., *Barron spaces and the compositional function spaces for neural network models*, arXiv preprint arXiv:1906.08039, (2019).

- [48] A. MANZONI, F. NEGRI, AND A. QUARTERONI, *Dimensionality reduction of parameter-dependent problems through proper orthogonal decomposition*, Annals of Mathematical Sciences and Applications, 1 (2016), pp. 341–377.
- [49] J. MARTIN, L. C. WILCOX, C. BURSTEDDE, AND O. GHATTAS, *A stochastic Newton MCMC method for large-scale statistical inverse problems with application to seismic inversion*, SIAM Journal on Scientific Computing, 34 (2012), pp. A1460–A1487, <https://doi.org/10.1137/110845598>.
- [50] P. G. MARTINSSON AND J. TROPP, *Randomized Numerical Linear Algebra: Foundations & Algorithms*, arXiv preprint arXiv:2002.01387, (2020).
- [51] F. MONTI, D. BOSCAINI, J. MASCI, E. RODOLA, J. SVOBODA, AND M. M. BRONSTEIN, *Geometric deep learning on graphs and manifolds using mixture model cnns*, in Proceedings of the IEEE Conference on Computer Vision and Pattern Recognition, 2017, pp. 5115–5124.
- [52] T. O’LEARY-ROSEBERRY, *hessianlearn: Stochastic Nonconvex Optimization in TensorFlow and keras*, 2021, <https://doi.org/10.5281/zenodo.4608644>, <https://github.com/tomoleary/hessianlearn>.
- [53] T. O’LEARY-ROSEBERRY, N. ALGER, AND O. GHATTAS, *Inexact Newton methods for stochastic non-convex optimization with applications to neural network training*, arXiv preprint arXiv:1905.06738, (2019).
- [54] T. O’LEARY-ROSEBERRY, N. ALGER, AND O. GHATTAS, *Low Rank Saddle Free Newton: Algorithm and Analysis*, arXiv preprint arXiv:2002.02881, (2020).
- [55] T. O’LEARY-ROSEBERRY AND U. VILLA, *hippyflow: Dimension reduced surrogate construction for parametric PDE maps in Python*, 2021, <https://doi.org/10.5281/zenodo.4608729>, <https://github.com/hippylib/hippyflow>.
- [56] M. T. PARENTE, J. WALLIN, B. WOHLMUTH, ET AL., *Generalized bounds for active subspaces*, Electronic Journal of Statistics, 14 (2020), pp. 917–943.
- [57] N. PETRA, J. MARTIN, G. STADLER, AND O. GHATTAS, *A computational framework for infinite-dimensional Bayesian inverse problems, part ii: Stochastic Newton MCMC with application to ice sheet flow inverse problems*, SIAM Journal on Scientific Computing, 36 (2014), pp. A1525–A1555.
- [58] R. PINNAU, *Model reduction via proper orthogonal decomposition*, in Model order reduction: theory, research aspects and applications, Springer, 2008, pp. 95–109.
- [59] A. QUARTERONI, A. MANZONI, AND F. NEGRI, *Reduced basis methods for partial differential equations: an introduction*, vol. 92, Springer, 2015.
- [60] L. RUTHOTTO, S. J. OSHER, W. LI, L. NURBEKYAN, AND S. W. FUNG, *A machine learning framework for solving high-dimensional mean field game and mean field control problems*, Proceedings of the National Academy of Sciences, 117 (2020), pp. 9183–9193.
- [61] C. SCHWAB AND R. A. TODOR, *Karhunen–Loève approximation of random fields by generalized fast multipole methods*, Journal of Computational Physics, 217 (2006), pp. 100–122.
- [62] C. SCHWAB AND J. ZECH, *Deep learning in high dimension: Neural network expression rates for generalized polynomial chaos expansions in UQ*, Analysis and Applications, 17 (2019), pp. 19–55.
- [63] M. SUGANUMA, S. SHIRAKAWA, AND T. NAGAO, *A genetic programming approach to designing convolutional neural network architectures*, in Proceedings of the Genetic and Evolutionary Computation Conference, ACM, 2017, pp. 497–504.
- [64] U. VILLA, N. PETRA, AND O. GHATTAS, *hIPPYlib: An extensible software framework for large-scale inverse problems*, The Journal of Open Source Software, 3 (2018), p. 940.
- [65] U. VILLA, N. PETRA, AND O. GHATTAS, *hIPPYlib: An Extensible Software Framework for Large-Scale Inverse Problems Governed by PDEs; Part I: Deterministic Inversion and Linearized Bayesian Inference*, Transactions on Mathematical Software, in print (2020), <https://arxiv.org/abs/1909.03948>.
- [66] K. WILLCOX AND J. PERAIRE, *Balanced model reduction via the proper orthogonal decomposition*, AIAA journal, 40 (2002), pp. 2323–2330.
- [67] K. WU, P. CHEN, AND O. GHATTAS, *A fast and scalable computational framework for large-scale and high-dimensional Bayesian optimal experimental design*, arXiv preprint arXiv:2010.15196, (2020).
- [68] D. XIU AND G. E. KARNIADAKIS, *The Wiener-Askey polynomial chaos for stochastic differential equations*, SIAM Journal on Scientific Computing, 24 (2002), pp. 619–644.
- [69] X. YAO, *Evolutionary artificial neural networks*, International journal of neural systems, 4 (1993), pp. 203–222.
- [70] O. ZAHM, P. G. CONSTANTINE, C. PRIEUR, AND Y. M. MARZOUK, *Gradient-based dimension reduction of multivariate vector-valued functions*, SIAM Journal on Scientific Computing, 42 (2020), pp. A534–A558.

- [71] Y. ZHU, N. ZABARAS, P.-S. KOUTSOURELAKIS, AND P. PERDIKARIS, *Physics-constrained deep learning for high-dimensional surrogate modeling and uncertainty quantification without labeled data*, Journal of Computational Physics, 394 (2019), pp. 56–81.

Appendix A. Scalable Computation of the Input and Output Projectors.

The matrices $\mathbb{E}_\nu[\nabla q^T \nabla q]$, $\mathbb{E}_\nu[qq^T]$ can be approximated in a scalable and efficient manner using sampling and matrix-free randomized linear algebra. The integrals for $\mathbb{E}_\nu[\nabla q^T \nabla q]$, $\mathbb{E}_\nu[qq^T]$ can be approximated as finite sums via Monte Carlo approximation; given draws $m_i \sim \nu$, one can generate training data $\{(m_i, q_i)\}_{i=1}^{N_{\text{data}}}$, and approximate the POD basis via Monte Carlo approximation:

$$(A.1) \quad \mathbb{E}_\nu[qq^T] \approx \frac{1}{N_{\text{data}}} \sum_{i=1}^{N_{\text{data}}} q_i q_i^T \in \mathbb{R}^{d_Q \times d_Q} = \Phi D \Phi^T.$$

A calculation of a low rank approximation of $\Phi D \Phi^T$ from samples is referred to as the method of snapshots since the training data q_i are taken to be “snapshots” of the outputs. The integral $\mathbb{E}_\nu[\nabla q^T \nabla q] \in \mathbb{R}^{d_M}$ can also be approximated via the action of the matrices on Gaussian random vectors. The integral approximation is obtained via Monte Carlo, for $\omega_M \in \mathbb{R}^{d_M}$:

$$(A.2) \quad \mathbb{E}_\nu[\nabla q^T \nabla q] \omega_M \approx \frac{1}{N_{\text{data}}} \sum_{i=1}^{N_{\text{data}}} \nabla q(m_i)^T \nabla q(m_i) \omega_M$$

This matrix-free computation requires the action of operators $\nabla q(m_i) \in \mathbb{R}^{d_Q \times d_M}$ and $\nabla q(m_i)^T \in \mathbb{R}^{d_M \times d_Q}$ at various points $m_i \in \mathbb{R}^{d_M}$. The Monte Carlo sum leverage modern computing architecture and use sample parallelism, making the computation for many samples tractable in terms of time and memory.

A.1. Approximation with randomized linear algebra. The single pass randomized eigenvalue decomposition algorithms can approximate the k low rank eigenvalue decomposition of a matrix $Q_k D_k Q_k^T \approx A \in \mathbb{R}^{n \times n}$ for $k + p$ matrix vector products, with expected approximation error bounded by

$$(A.3) \quad \mathbb{E}_\rho[\|A - Q_k D_k Q_k^T\|] \leq \left(1 + 4 \frac{\sqrt{n(k+p)}}{p-1}\right) |d_{k+1}|.$$

See [40, 50], More accuracy can be obtained via double pass or power iteration, but this requires more applications of the operators. Here \mathbb{E}_ρ denotes the expectation taken with respect to the Gaussian measure ρ from which the random matrix $\Omega \in \mathbb{R}^{n+(k+p)}$ is sampled. Higher accuracy in the approximation can be achieved for more applications of the operator (i.e. power iteration, multi-pass methods). Automated procedures such as adaptive range finding can be used to find the rank k such that a specific tolerance is met, i.e. for a given $\epsilon > 0$ find k, p such that

$$(A.4) \quad \left(1 + 4 \frac{\sqrt{n(k+p)}}{p-1}\right) |d_{k+1}| \leq \epsilon.$$

The matrix approximation is formed via the action of the operator on Gaussian random vectors which is guaranteed to resolve dominant modes of the operator due to concentration of measure, matrix concentration inequalities such as Bernstein or Chernov. This is an inherently scalable process since all of the matrix vector products

are independent of one another, i.e. they can be efficiently parallelized and high levels of concurrency can be leveraged. This is in contrast to other matrix-free approximations such as Krylov, where the matrix vector products are inherently serial.

A.2. The action of ∇q and ∇q^T using adjoints. The implicit derivative of the outputs $q(m) = q(u(m))$ with respect to the parameters m can be found via a Lagrange multiplier approach to incorporate the implicit dependence on the weak form of the state equation. Since $q(m) \in \mathbb{R}^{d_Q}$, the result is derived for each component:

$$(A.5) \quad \mathcal{L}_i(u, m, v) = q(u(m))_i + v_i^T R(u, m),$$

or equivalently take all derivatives at once, with the adjoint variable matrix $V \in \mathbb{R}^{d_V \times d_Q}$:

$$(A.6) \quad \mathcal{L}(u, m, v) = q(u(m)) + V^T R(u, m).$$

A variation of \mathcal{L} with respect to the adjoint variable matrix yields the state equation:

$$(A.7) \quad R(u, m) = 0,$$

which is solved for u , given a draw m . A variation of \mathcal{L} with respect to the state variable u yields the adjoint equation:

$$(A.8) \quad \underbrace{\frac{\partial q}{\partial u}}_B + V^T \underbrace{\frac{\partial R}{\partial u}}_A = 0$$

which is solved for each adjoint variable:

$$(A.9) \quad V^T = -BA^{-1}.$$

Lastly a variation of \mathcal{L} with respect to the parameters m allows for the formation of the Jacobian:

$$(A.10) \quad \nabla_m q + V^T \underbrace{\frac{\partial R}{\partial m}}_C = 0.$$

So finally one can compute

$$(A.11) \quad \nabla_m q(u(m)) = BA^{-1}C = \frac{\partial q}{\partial u} \left[\frac{\partial R}{\partial u} \right]^{-1} \frac{\partial R}{\partial m}.$$

To evaluate at a point m_i one must solve the state and adjoint equations first before applying the operator in a direction $\hat{m} \in \mathbb{R}^{d_M}$:

$$(A.12) \quad \nabla_m q(u(m_i))\hat{m} = BA^{-1}C\hat{m}.$$

The state and adjoint equations only need to be calculated once before the action of the operator in many directions \hat{m} is formed. Similarly the transpose of the operator can be applied to $q \in \mathbb{R}^{d_Q}$ via

$$(A.13) \quad \nabla_m q(u(m))^T = C^T A^{-T} B^T \hat{q}.$$

The key observation about the action of ∇q and ∇q^T is that unlike the forward solution of the PDE state equation they do not involve any nonlinear iterations. These operators only involve linearizations of the PDE. These matrices can be efficiently computed and applied over and over to many right hand sides, which makes the cost of evaluating the derivatives via adjoint methods cheaper than the forward solution of the parametric PDE. The expensive part of the derivative evaluation is the solution of the forward nonlinear PDE, which is required for training data generation anyways. Thus one can save computation by generating training data and approximations of derivative subspaces in tandem. The computational cost of computing derivative subspaces of the outputs is marginally less expensive than the evaluation of the nonlinear mapping. The costs of the linearizations can be made negligible in regimes where direct solvers is used for the forward mapping, or iterative solvers with preconditioners are used. In the case of a direct solver, the matrix factorization costs can be amortized when applied to many different right hand sides. When an iterative solver with a preconditioner is used, the action of the preconditioner and its transpose can be reused to evaluate the action of ∇q and ∇q^T .

Appendix B. Numerical Experiment Appendix.

B.1. Notes on implementation specifics. A complete description of parametric PDEs and neural networks can be found in <https://github.com/hippylib/hippyflow>. For the convection-diffusion-reaction problem 256 samples were used in the Monte Carlo approximation for the active subspace projector. For the Helmholtz problem 128 were used. For both convection-diffusion-reaction and Helmholtz problems 400 samples were used in the Monte Carlo approximation of the proper orthogonal decomposition. No sampling was required for the KLE projector computation.

The AS and KLE projectors in `hIPPYflow` are covariance matrix and mass matrix orthogonal respectively. This makes the computation of these projectors consistent in the infinite dimensional limit. Numerical results for the neural network approximation were improved however when these projectors were re-orthogonalized with respect to the identity matrix. Rescaling also improved the numerical results. See <https://github.com/hippylib/hippyflow> for more information.

Gradient and Hessian subsampling were used to improve both the performance and computational cost of the inexact Newton CG optimizer. When the number of training data were greater than or equal to 256, a gradient batch size of 128 was used and a Hessian batch size of 16 was used. When the batch size was less than 256, a gradient batch size of $N_{\text{data}}/4$ was used, and a Hessian batch size of $N_{\text{data}}/32$ was used. For more information on gradient and Hessian subsampling see [53].

Unregularized least squares led to better testing accuracy in this problem (probably need surgical regularization that leaves the informed modes unchanged). In order to improve the conditioning of the CG solve in Inexact Newton CG, Levenberg-Marquardt damping of $\gamma = 10^{-3}$ was used. For information on the implementation specifics of the optimizer, see <https://github.com/tomoleary/hessianlearn>.

B.2. Distribution for uncertain parameters m . Both problems use a Gaussian probability distribution for the uncertain parameters m , with Matérn covariance that is a fractional PDE operator:

$$(B.1) \quad C = (\delta I - \gamma \nabla \cdot (\Theta \nabla))^{-\alpha}.$$

The uncertain parameters m are the solution of a linear fractional stochastic PDE [45]. The choice of $\alpha > d/2$ where d is the spatial dimension of the PDE, makes the

covariance trace class, in both problems we take $\alpha = 2$. When the covariance is trace class this guarantees that the uncertain parameters m is L^2 integrable, which makes the PDE well-posed. This trace class condition is also typically required for the well-posedness of outer loop inference problems that the surrogate is to be used in. The coefficients $\delta, \gamma > 0$ that show up in the fractional PDE control the correlation length as well as the marginal variance of the probability distribution (i.e. the difficulty of the problem). The matrix $\Theta \in \mathbb{R}^{d \times d}$ introduces spatial anisotropy [31]. When the PDE problem is discretized the vector representation of m has dimension d_M and we consider m to be a vector in \mathbb{R}^{d_M} .

The correlation length for draws from ν is controlled by the ratio δ/γ , and for a fixed correlation length, larger values of γ and δ reduce the marginal variance for distribution.

B.3. Convection-Diffusion-Reaction PDE Problem. The volumetric forcing function \mathbf{f} is a Gaussian bump located at $x_1 = 0.7, x_2 = 0.7$.

$$(B.2) \quad \mathbf{f}(x, y) = \max \left(0.5, e^{-25(x_1-0.7)^2 - 25(x_2-0.7)^2} \right)$$

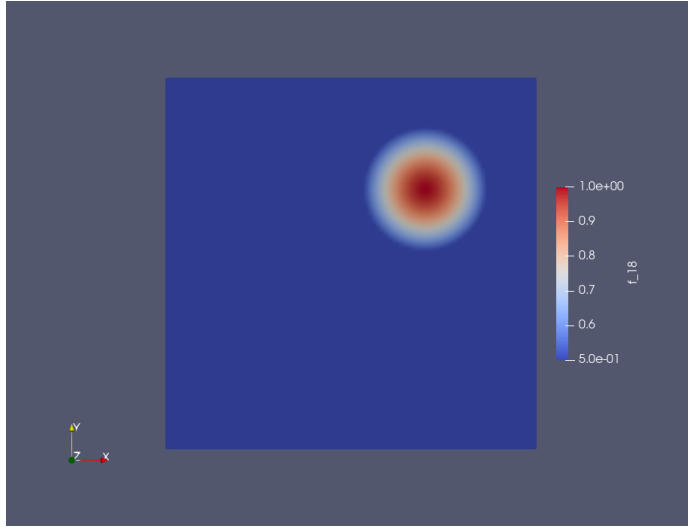


Fig. 16: Truncated Gaussian blob forcing term

The velocity field \mathbf{v} used for each simulation is the solution of a steady-state Navier-Stokes equation with side walls driving the flow:

$$(B.3a) \quad -\frac{1}{Re} \Delta \mathbf{v} + \nabla q + \mathbf{v} \cdot \nabla \mathbf{v} = 0 \text{ in } \Omega$$

$$(B.3b) \quad \nabla \cdot \mathbf{v} = 0 \text{ in } \Omega$$

$$(B.3c) \quad \mathbf{v} = \mathbf{g} \text{ on } \partial\Omega.$$

The coefficient $Re = 100$ is the Reynolds number, and the Dirichlet term \mathbf{g} is given by $\mathbf{g} = \mathbf{e}_2$ on the left wall, $\mathbf{g} = -\mathbf{e}_2$ on the right wall and zero everywhere else (see the

Advection-Diffusion Bayesian Tutorial in hIPPYlib for more information [64]). The velocity field is shown below.

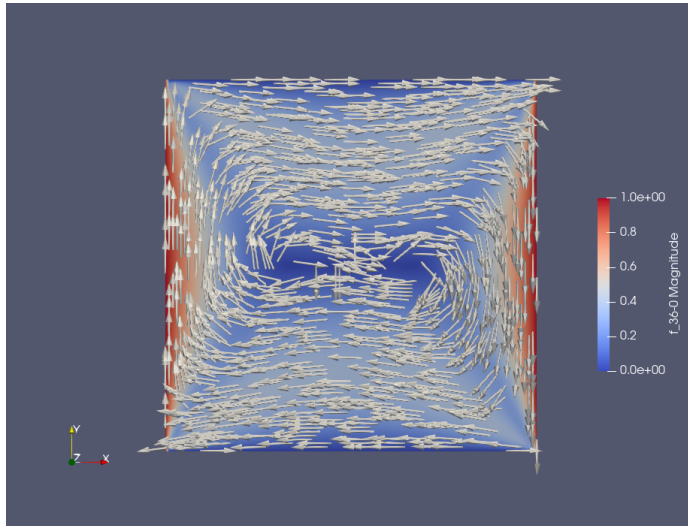


Fig. 17: Velocity field for convection-diffusion-reaction PDE